International Journal of Naval Architecture and Ocean Engineering 15 (2023) 100530

Contents lists available at ScienceDirect

International Journal of Naval Architecture and Ocean Engineering

journal homepage: http://www.journals.elsevier.com/international-journal-of-naval-architecture-and-ocean-engineering/

Potential energy savings of air lubrication technology on merchant ships

Young-Rong Kim*, Sverre Steen

Department of Marine Technology, Norwegian University of Science and Technology (NTNU), Trondheim, Norway

ARTICLE INFO

Article history:
Received 24 January 2023
Received in revised form
12 April 2023
Accepted 15 April 2023
Available online 1 May 2023

Keywords:
Air lubrication system
Drag reduction
Energy saving
Fleet-level analysis
Ship transportation

ABSTRACT

As the reduction of greenhouse gas emissions has become an important issue, measures and devices to reduce energy consumption are in increasing demand. In this study, the potential energy saving due to the application of air lubrication technology in merchant ships is analyzed. We propose a simplified empirical model, covering three different air lubrication technologies, based on the experimental results and assumptions taken in the existing studies. The bottom surface area covered with air is important for the efficiency of the air lubrication system, according to the sensitivity analysis. From the global fleet analysis, net-percentage power saving varies according to the operational profile as well as the technology. Net-percentage power savings of 2–5% from air bubble, 8–14% from air layer, and 16–22% from air cavity technology were obtained assuming calm-water conditions. The methodology can be adopted in early design stage and fleet-wide analyses of various energy-saving measures.

1. Introduction

Along with the acceleration of global warming, the international community is paying keen attention to greenhouse gas emissions. The International Maritime Organization (IMO) released an initial strategy, which aims to reduce greenhouse gas emissions by at least 50% in shipping by 2050 compared to 2008 levels and reduces emissions in stages as soon as possible, at Marine Environment Protection Committee (MEPC 72) in 2018 (IMO, 2018). In addition, IMO adopted EEXI (Energy Efficiency eXisting Ship Index) and CII (Carbon Intensity Indicator) as direct and short-term measures for this (IMO, 2021). In response to this international trend, various types of energy-saving devices and measures have been studied and applied to ships (Bouman et al., 2017; Zhang et al., 2021).

Air Lubrication Systems (ALS) have been proposed as a promising energy-saving technology that can effectively lower fuel consumption and greenhouse gas emissions from ships. Frictional resistance generally accounts for the largest portion of a ship's total resistance, especially in slow-moving ships, where it can account for more than 80% of the total. Air supplied from ALS to the bottom of the hull can reduce frictional resistance by reducing the effective wetted surface area of the vessel through lubrication between the water flow and the hull surface.

Mitsubishi Heavy Industry first installed its air lubrication system (MALS) on a newly built ship and showed up to 12% net energy savings in a sea trial of a module carrier (Mizokami et al., 2010). As the nominal thickness of the air layer that forms on the bottom of the hull increases, it has also been confirmed that net energy savings increase as well. In a subsequent study, Kawabuchi et al. (2011) analyzed the distribution of air bubbles on the hull surface and its effect on propeller performance using CFD. Silverstream developed an air carpet technology that covers the entire bottom of the ship by injecting micro bubbles from air release units, and it was confirmed that a net energy reduction of about 4% could be achieved from actual operations of 40 k DWT tanker (Silberschmidt et al., 2016). In Lee et al. (2017), they observed results from model tests, sea trials, and in-service data from two ships fitted with air-lubrication systems (SAVER) made by Samsung Heavy Industry (SHI). As a result, in the case of a heavy cargo carrier, power savings of 8.8% were estimated in the sea trial results, and on the basis of long-term trip data, power savings of roughly 4–5% were recorded for a LNG carrier. In the meantime, Damen group unveiled the Air Chamber Energy Saving (ACES) system, which uses a chamber-shaped design on the bottom of the hull to create a cavity where air is supplied to prevent water from coming into contact with the lower hull surface (Pavlov et al., 2020). According to several investigations (ABS, 2019; Gebraad et al., 2021), there have been about 50 ships with air lubrication

* Corresponding author.
E-mail address: youngrong.kim@ntnu.no (Y.-R. Kim).
Peer review under responsibility of The Society of Naval Architects of Korea.

https://doi.org/10.1016/j.ijnaoe.2023.100530

systems installed by 2021, including some test cases, and interest in the technology continues to increase considering recent orders.

Many previous studies have looked at the applicability and performance of air-lubrication systems for certain ship cases based on model tests, sea trials, or CFD. On the other hand, some studies have suggested a simplified method for estimating energy savings in the air lubrication system. Mäkiharju and Ceccio (2011), and Mäkiharju et al. (2012) established a method of calculating the energy economy of the air lubrication system using experimental data and presented the energy-saving results based on the assumption of various situations for the U.S. Great Lakes vessel. Comer et al. (2019) applied a similar method to perform an analysis on route-based fuel and emission reduction of the three ships installed with ALS.

In this study, a simplified model, capable of applying different types of ALS considering various ship types and profiles, is presented. Through the suggested model, this study aims to assess the impact of ALS on different ship types and obtain knowledge to help reduce maritime emissions. The suggested model is intended for early-design estimations, fleet-wide studies, and similar applications where quick calculations requiring limited input are desired. The underlying idea for the simplified method is that the layer of air produced by the air lubrication system reduces frictional resistance by covering a portion of the hull's surface area with air, or air bubbles. In order to enable the evaluation of the effectiveness of air lubrication technology for ships with different design characteristics and operating profiles, the aforementioned simplified empirical approach is adopted. The model has been established based on previously published experimental results and various information found in open literature, and throughout this paper, the calculation process and basic assumptions are explained. It includes three types of air lubrication: air bubble, air layer, and air cavity.

In Chapter 2, the general concepts and different types of air lubrication systems are presented, and relevant studies used to develop the simplified method are also introduced. In the following chapter, the background of the various formulas employed in the model to calculate the potential savings of an air lubricating system is discussed. Additionally, by comparing the results of the model with those of other studies, the overall properties and performance are demonstrated. Chapter 4 presents the research outcomes based on the model that has been established. Here, parametric studies are performed on the main factors of an air lubrication system, and potential power savings for the global fleet in calm water and a specific vessel in the real sea are evaluated. The last chapter presents the conclusions obtained from the study and proposes future works.

2. Background

Frictional resistance often predominates among the resistance components that a ship encounters when moving through water, and it is heavily influenced by the wetted surface area, operating speed, and viscosity of the fluid. Basically, the main principle of air lubrication technology is to reduce frictional resistance by reducing direct contact with water, that is to reduce the wetted surface area by releasing air bubbles and covering some part of the bottom surface area of the hull. Air lubrication can be classified into three different techniques; the air bubble concept that injects micro air bubbles at the bottom of the hull, the air film concept covers the bottom surface with a continuous air layer through increased air flux, and the air cavity concept fills the recessed area beneath the hull with air (Foeth et al., 2009; ABS, 2019). In the rest of the text, air bubble concept will be referred to as BDR (Bubble drag redction), air film as ALDR (Air layer drag reduction), and air cavity as PCDR (Partial cavity drag reduction).

BDR reduces the local density by injecting numerous micro-bubbles into the boundary layer, thereby reducing the Reynolds stress. At the same time, the effective viscosity is reduced due to an increase in void fraction, which consequently serves to suppress the turbulence of the flow and reduce skin friction (Park and Lee, 2018; ABS, 2019). As the injected air flux increases from this state, a transition occurs in which the air bubbles and the air layer coalesce with each other in the gas-liquid mixture. When sufficient air is injected into the near wall region of the turbulent boundary layer, the air is aggregated with each other to form a continuous air layer separating the hull surface from the water flow. It was found that such a developed air layer, so-called ALDR can significantly reduce frictional resistance compared to bubbly flow (Ceccio, 2010; Elbing et al., 2013). PCDR reduces frictional resistance by injecting air into a recess or cavity at the bottom of the hull to separate the lower part of the hull from water (Lay et al., 2010). A typical hull design for PCDR consists of a slightly downward sloping closure downstream from the starting wall of the cavity into which air is injected, which forms a partial cavity to trap the air. This drag reduction effect by the cavity air layer is associated with the design of the bottom cavity and the continuous injection of air to maintain a stable air layer (Wu and Ou, 2019).

To analyze the impact of an air lubrication system on the speed-power performance of a ship and to get insight into the optimal hull design and arrangement of the air lubrication system, several methods such as a model test, full-scale measurements, and CFD computation are typically used. Fig. 1 presents the net-percentage power savings of each air lubrication system collected from these studies as a horizontal box plot, along with a scatter plot of the collected data. Several studies have used various metrics such as fuel consumption, gas emission, drag reduction, and power saving, but since net-percentage power savings defined in Eq. (1) will be used as a performance metric of ALS throughout this study, only the results that can estimate such value are presented here, and the detailed sources are presented in Table A.1 in appendix A. Although each experiment was classified and listed by ALS type, some experiments may correspond to a transitional region depending on the injected airflow. According to the 25%–75% quartile ranges corresponding to both ends of the box, BDR indicates a net-percentage power saving of about 3–6%, ALDR of 4–12%, and PCDR of 16–22%. It is clear that there are scatters in any type of air lubrication because the effectiveness of power savings is highly dependent on the operational profiles of the ship, the details of the air lubrication arrangement, and the experimental setup.

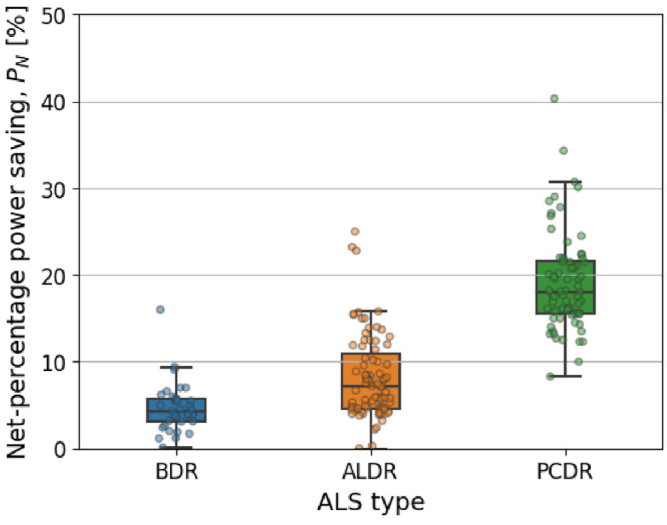

Fig. 1. Potential net-percentage power savings achieved from previous studies. The detailed data sources are listed in Table A.1.

3. Methodology

3.1. Modeling of air lubrication technology

The purpose of the method developed in this study is to evaluate the potential energy saving of air lubrication systems on merchant ships and to obtain practical knowledge through the obtained results. It is anticipated that the applicability of air lubrication technology will vary because ships operating globally have diverse design characteristics and operating profiles. Since it is an analysis of a wide variety of general-purpose levels, it is necessary to develop a model that can simulate the overall trend in energy savings using the fundamental ship information. Therefore, the energy economic calculation approach used in Mäkiharju et al. (2012) was adopted in this study as the performance evaluation method of ALS, and required volumetric fluxes of gas for the air-lubrication were estimated based on experimental data obtained from large cavitation tunnel in Elbing et al. (2008) and Makiharju et al. (2010). In addition, a number of assumptions and simplifications were made regarding the application and composition of the air lubrication system based on the findings of earlier studies that were published.

3.1.1. Energy saving by air lubrication system

The energy savings by the air lubrication system are determined by the reduction of the power required to overcome the frictional drag on the lubricated surface and the power consumed to inject gas into the bottom surface. Here, the performance index of the air lubrication system uses the percentage of net power saving to total brake power, that is, net-percentage power saving, as stated in Eq. (1). The total resistance and overall efficiency can be used to estimate the total brake power, as shown in Eq. (2).

$$P_N[\%] = \frac{P_{save} - P_{cons}}{P_B} \times 100 = \frac{P_{net}}{P_B} \times 100 \tag{1}$$

$$P_B = \frac{R_T \times V}{\eta_T} \tag{2}$$

where P_N is net-percentage power saving, P_{save} is power saved by air lubrication system; it can be replaced by $P_{save,wc}$ if there is an influence of weather, P_{cons} is power consumed by air compressor, P_{net} is net power saving by air lubrication system, P_B is total brake power, R_T is total resistance in real sea conditions, η_T is overall efficiency, and V is ship speed.

The total resistance in real sea conditions can be simply expressed as Eq. (3), and it is considered as the sum of the calm water resistance and the additional resistance caused by wind and waves. Here, it is possible to estimate each of the resistance components that make up the ship's total resistance using established empirical methods, and the methods used in this study are listed in Table 1.

$$R_T = R_{Calm} + R_{Wind} + R_{Wave} \tag{3}$$

where R_{Calm} is total resistance in calm water conditions, R_{Wind} is added resistance due to wind, and R_{Wave} is added resistance in waves.

For the estimation of the calm water resistance of a ship, it can be estimated from various methods listed in Table 1 to suit the dimensions and operating range of each ship. To use wind resistance coefficients taking into account different ship types and windage area above the waterline, wind tunnel test results from Blendermann (1996), Fujiwara (2006), and ISO (2015) were gathered. Moreover, the Combined Method, by Kim et al. (2022b) is used in the model to compute the added resistance in arbitrary wave headings using a few basic inputs. In order to obtain the propulsive efficiency for various ships, this study uses the simplified method (Kristensen and Lützen, 2012), which can obtain a quick estimate from Wageningen B-series (Oosterveld and Van Oossanen, 1975) using a limited input value, and the methods found in Birk (2019). In Nagamatsu et al. (2002)'s full-scale experiment, a bubble injector was dedicatedly designed to prevent the decrease in propeller efficiency due to the inflow of air bubbles into the propeller. However, according to later studies (Kawakita et al., 2011; Kawabuchi et al., 2011; Jang et al., 2014), the loss of propulsive efficiency before and after starting the air lubrication system was less than about 1%, demonstrating that air bubbles may not have much of an impact on a propeller. Based on this fact and for the simplicity of the model, this study neglect to include any change in propulsive efficiency caused by air bubbles.

In Section 5, the resistance of different commercial ships in the global fleet is estimated. The resistance is calculated using the well-established empirical methods listed in Table 1. A method for selection of the best empirical methods for each ship has been established (Kramel et al., 2021). In the fleetwide calculation in this work, an updated version is applied, where some additional empirical methods are included, as listed in Table 1. The main feature of this resistance calculation method is that it requires few input parameters. If more detailed information is available, more advanced resistance prediction methods can be applied.

3.1.2. Power saving by the air lubrication

The air lubricating device serves to reduce the resistance of the area covered with air on the bottom surface among the frictional resistance generated from the fluid surrounding the hull during ship operation. Therefore, the power that can be saved from the air lubrication can be calculated by simply taking into account the power due to the frictional resistance generated by the wetted surface area, the proportion of the air covered area to the total wetted surface, and the drag reduction achieved by the air covered area, as shown in Eq. (4).

$$P_{save} = P_F D_R \frac{A_a}{A_w} \tag{4}$$

where P_F is the power required to overcome the frictional drag, D_R is frictional drag reduction fraction due to air lubrication, A_a is air covered area at the bottom surface, and A_w is wetted surface area.

As in Eq. (5), the power needed to overcome the frictional drag can be obtained by multiplying the total brake power by the

Table 1
Estimation of resistance components using empirical methods used in the study.

Component	Method
R_{Calm}	Holtrop-Mennen (Holtrop and Mennen, 1982), Hollenbach (Hollenbach, 1998), Guldhammer (Guldhammer and Harvald, 1974; Kristensen and Lützen, 2012), Oortmerssen (Van Oortmerssen, 1971; Helmore, 2008)
R_{Wind}	Blendermann (Blendermann, 1996), Fujiwara (Fujiwara, 2006), STAJIP (ISO, 2015)
R_{Wave}	Combined Method (Kim et al., 2022b)
η_T	Kristensen (Oosterveld and Van Oossanen, 1975; Kristensen and Lützen, 2012), Birk (Birk, 2019)

proportion of frictional drag to total drag. Here, the frictional drag coefficient of the flat plate can be calculated using the ITTC 1957 friction line (ITTC, 1978) from Eq. (7), and accordingly, the frictional resistance is obtained from Eq. (6). As indicated in Eq. (3), the total resistance can be determined from empirical methods.

$$P_F = P_B \times \frac{R_F}{R_T} \tag{5}$$

$$R_F = \frac{1}{2}\rho_w A_w C_F V^2 \tag{6}$$

$$C_F = \frac{0.075}{(\log_{10} R_n - 2)^2} \tag{7}$$

where ρ_w is water density, R_F is frictional resistance, C_F is frictional coefficient, and R_n is Reynolds number.

According to Silberschmidt et al. (2016), the estimated appendage drag of the air release units attached to the bottom surface of LNG carriers or cruise ships was less than 0.5% of the total. In this study, the influence of appendages for all ALS types is ignored for simplicity, and in the case of PCDR, it is assumed that there is a newly built ship with proper design alterations for the cavity form. By ignoring appendage drag for the ALS, it is in fact assumed that great care has been taken to design the ALS in a careful way.

Among the wetted surface areas under the waterline of a ship, the air covered area, which can be expected to reduce frictional resistance by the air lubrication system, is expressed in the form of A_a/A_w as shown in the following Eq. (8) to facilitate calculation in this study. Here, wetted surface area, bottom area, and air covered area are defined as shown in Fig. 2. The area that can be covered with air bubbles or layers increases as the flat bottom surface of the hull increases. This implies that the potential energy saving from the air lubrication grows.

The bottom area of a ship can be estimated from the particular hull shape of the ship, but as it is nearly impossible to get comprehensive hull shape data for ships at the fleet level, this study proposed regression equations to estimate the bottom area of a ship (refer to Eq. (9)). They have been developed based on 22 ships with various hull shapes (refer to Table A.2 in appendix A), and presented the ratio of bottom surface area to wetted surface area (A_b/A_w) according to draught ratio (T/T_d) and block coefficient (C_b) as illustrated in Fig. 3. Here, C_b is based on the design draught of the ship. It is obvious that the A_b/A_w rises as C_b increases, and the A_b/A_w of the ballast condition is higher than that of the laden condition. For bulk carrier and tankers with normally blunt hull shapes, the flat bottom area tends to be bigger, whereas, for container ships and ferries with typically slender hull shapes, it tends to be smaller.

$$\frac{A_a}{A_w} = \frac{A_b}{A_w}\frac{A_a}{A_b} \tag{8}$$

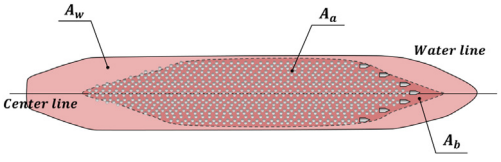

Fig. 2. Bottom-up view showing air covered area, bottom area, and wetted surface area of a ship.

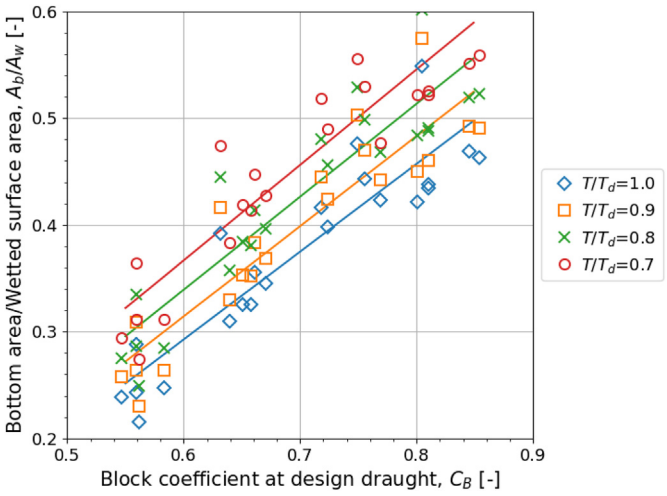

Fig. 3. The ratio of bottom area to wetted surface area according to C_b of a ship at various draught.

$$\frac{A_b}{A_w} = \begin{cases} 0.8227C_b - 0.201 & T/T_d = 1.0 \\ 0.8449C_b - 0.1927 & T/T_d = 0.9 \\ 0.871C_b - 0.1834 & T/T_d = 0.8 \\ 0.8942C_b - 0.1698 & T/T_d = 0.7 \end{cases} \tag{9}$$

where A_b is bottom surface area of a ship, C_b is block coefficient, T is sailing draught, and T_d is design draught.

Meanwhile, the arrangement of the air release device and the hull bottom design of the specific ship may affect the air covered area. Kim et al. (2021) found that the reduction rate of frictional resistance gradually increased as the air injection holes were placed wider in the width direction, and Park and Lee (2018) reported that it was more effective to inject air distributedly in multiple locations than in a single injection location. In this regard, it is important to appropriately arrange the injectors to increase the covering area of air at the bottom of the hull as much as possible. Based on the result in Wu and Ou (2019), 0.84 was used as a ratio of air covered area to the bottom area (A_a/A_b) in this study. However, this value can be changed as needed depending on each ship's ALS configurations.

Fig. 4 depicts the boundaries for three drag reduction regions based on flow rate in the air bubble injection experiment on the flat plate as given in Elbing et al. (2008). According to the flow rate, I represents the BDR region, II the transitional region between the BDR and ALDR, and III the ALDR region. The transitional gas injection rate for BDR (q_{trans}) and the critical gas injection rate for ALDR (q_{crit}) are indicated by the vertical lines in the figure. In region I, when air is injected into the bottom surface of the hull, the flow of air-liquid mixture predominates at the turbulent boundary. As the air flux gradually increases, some air bubbles are combined to form a partial air layer, and a transition in which the mixed flow and the air layer coexist occurs (q_{trans}). Here, in region II, as the air flux increases, the frictional drag reduction starts to rapidly increase from 20% to 80%. When the air flux exceeds the critical value (q_{crit}), a continuous air layer is completely developed, and the drag reduction is 80% or more.

The drag reduction values shown in Fig. 4 were measured at a location of 6.05 m in the streamwise direction from the air injector at the bottom of the plate, which is approximately half the length of the entire plate. In fact, as the bubbles move toward the downstream direction, the sizes of the bubbles change due to the coalescences and splits or the bubbles escape from the near wall boundary layer, thereby reducing the drag reduction effect (Kodama et al., 2005; Elbing et al., 2008; Verschoof et al., 2016). In some studies, endplates were installed along the entire length to

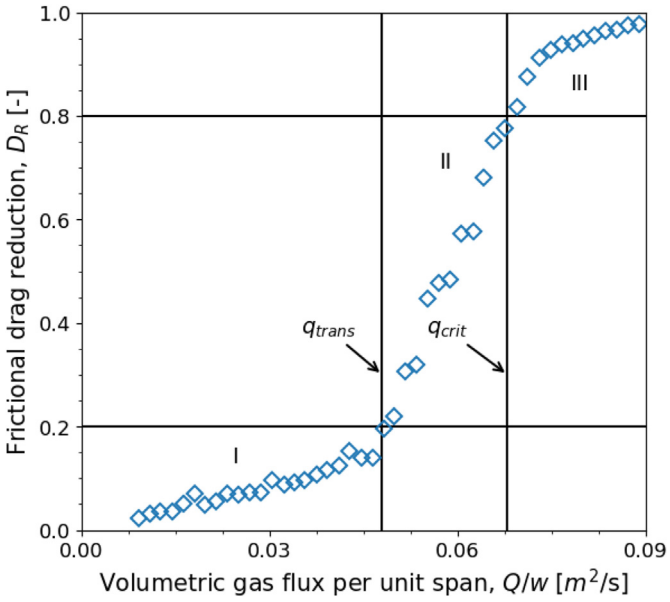

Fig. 4. Drag reduction of three regions according to the gas injection rate measured from the model tests on the flat-plate. I, II, and III represent BDR region, transition region between BDR and ALDR, and ALDR region, respectively. The figure is adapted from Elbing et al. (2008) with minor modifications.

trap the air bubble in the bottom to achieve an effect (Kawashima et al., 2007; Hoang et al., 2009). As such, it is very important to maintain the continuity of air bubbles at the bottom of the hull. It is assumed that the generated air layer persists along the bottom of the hull with the bubbles evenly distributed and maintaining the level of drag reduction at the certain air flux measured in the experiment. These experimental results were used as a criterion for designing the ALS model in this study, and thus a drag reduction of 20% in the transition region of BDR and 80% in the critical region of ALDR were assumed. Since the cavity closure has a drag reduction of more than 95% once it has been completed, as per Lay et al. (2010)'s analysis, a conservative 95% is used for the PCDR here. In other words, the relevant fixed drag reduction value and the air flux necessary under specified circumstances for each type of ALS are employed as indicated in Fig. 4. However, in model tests or real ships injected with different air flow rates, it is anticipated that a slightly varying drag reduction may be attained.

3.1.3. Power consumption by air compressor

An air compressor or blower must be used to send air to the outlet nozzles at the bottom of the hull in order to form and maintain an air bubble layer beneath the ship's surface. The power used by the compressor varies according to the pressure and volume of air transferred, which has a significant impact on the real gain of an air lubrication system. According to Buckingham and Pearson (2019), using compressor manufacturer data may be more accurate in estimating compressor power consumption, but in this paper, keeping simplicity and versatility prioritized, the power needed to compress the gas at a specified mass flow rate is determined using the polytropic process (Mäkiharju et al., 2012), as shown in Eqs. (10)-(11). The expansion or compression process including heat transfer is approximately described by the polytropic process equation (Nag, 2013).

$$P_{cons} = \frac{P_{comp}}{\eta_e} \tag{10}$$

$$P_{comp} = \frac{\dot{m}_g}{\eta_c \rho_1} P_1 \frac{n}{n-1} \left(\left[\frac{P_2}{P_1} \right]^{\frac{n-1}{n}} - 1 \right) \tag{11}$$

where P_{comp} is the power needed to compress a specified quantity of gas, η_e is the efficiency of electrical motor ($\eta_e = 0.9$), η_c is efficiency of an air compressor ($\eta_c = 0.6$), $\dot{m}_g$ is the mass flow rate of air necessary to maintain the given volume flow rate of air on the bottom surface, ρ_1 is the initial density of the air where it is compressed, P_1 is the atmospheric pressure, P_2 is the air delivery pressure from the compressor, and n is the polytropic index, chosen as the value valid for adiabatic processes ($n = 1.4$).

The pressure (P_2) required by the compressor to deliver air to the bottom of the hull to achieve air lubrication, consisting of static pressure and dynamic pressure of the bottom air inlet of the hull, and pressure loss due to the piping as shown in Eqs. (13)-(14). In general, since the hull is deeply submerged in water, the influence of static pressure contributes the most to the compressor power. The amount of pressure loss caused by piping losses varies on a number of factors, including the piping length, roughness, and the relevant design of the air lubrication system. Some of the existing articles calculated frictional pressure loss and minor loss from a moody chart assuming a certain pipe surface roughness (Mäkiharju et al., 2012; Comer et al., 2019), while others (Ceccio and Mäkiharju, 2012; Jang et al., 2014; Gallardo Martínez, 2016) used a range of 1–1.5 atm for the pressure drop due to piping losses. As a cautious estimate for the pressure drop caused by pipe, 1.5 atm was used in this study.

$$\dot{m}_g = qw \frac{\rho_1 P_3}{P_1} \tag{12}$$

$$P_2 = P_3 + \Delta P_{loss} \tag{13}$$

$$P_3 = \rho_w g T + \frac{1}{2} \rho_w V^2 \tag{14}$$

where q is the volumetric gas flux per unit span, w is the width of air covered area, P_3 is the pressure under the hull, ΔP_{loss} is pressure drop due to piping losses, and g is gravitational acceleration.

For the estimation of the volume flux of gas required to achieve a given air lubrication type beneath the hull, the experimental data of Elbing et al. (2008) and Makiharju et al. (2010) conducted in the large cavitation tank was used. Fig. 5 shows volumetric air flux per span (q) for each air lubrication type according to the flow rate measured from the experiments. In Elbing et al. (2008), air flux was converted to an air layer nominal thickness, and drag reduction according to thickness was used in their studies. In this model, as shown in Fig. 5, gas flux according to flow speed was used as reference data for calculating compressor power for each ALS type. In addition, the gas fluxes of the air lubrication system estimated from the sea trials of the bulk carrier and module carrier are also displayed (Hoang et al., 2009; Mizokami et al., 2010). According to Mäkiharju et al. (2012), these investigations hypothesize that an air layer or transitional region formed on the hull's bottom because the reduction in friction drag was lowered by 20–40%, which is partly compatible with the outcomes of Elbing et al. (2008), and Makiharju et al. (2010).

The air flux required to achieve the air layer or air cavity grows proportionally as the flow rate rises. In this study, BDR used q_{trans} in the transition region between BDR and ALDR with 20% drag reduction as in Fig. 4. The required air flux in the corresponding state is much less than the air flux for maintaining the ALDR at the smooth and rough plates. In the case of ALDR, the result was obtained in a state in which the q_{crit}, that is, the continuous air layer is

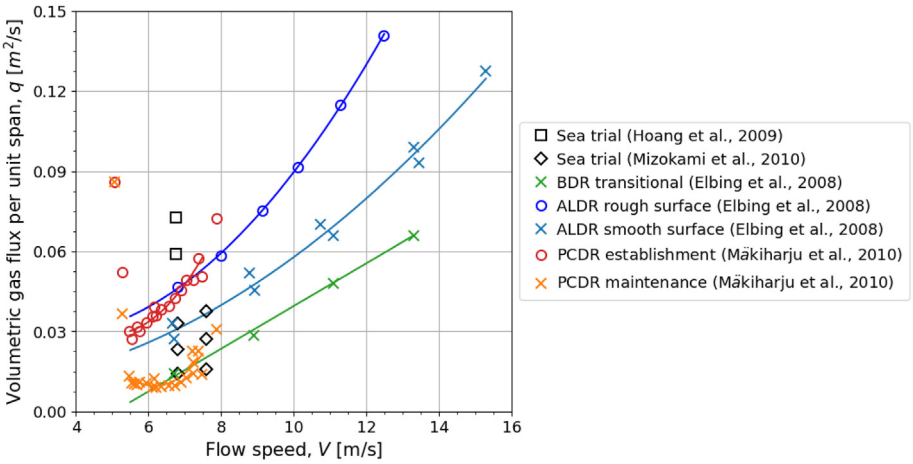

Fig. 5. The volumetric air flux per unit span required for different air lubrication techniques according to the flow speed. The figure is adapted from Mäkiharju et al. (2012) with minor modifications.

fully developed. It can be confirmed that the rough surface requires additional gas flux to achieve the same extent of frictional drag reduction as on the smooth surface. In the case of PCDR, it is separated into the gas flow necessary to establish or maintain the cavity, and the required airflow of them is significantly different (Mäkiharju et al., 2013). Since the gas flux needed to maintain the cavity is less than half that needed to generate it and is almost identical to the gas flux needed for the BDR, hence the power used by the compressor for the PCDR is actually very little.

According to Makiharju et al. (2010), in the flat plate experiment, the air cavity did not easily reach the beach (end of the closure) at a lower flow speed, and the flow in the cavitation tunnel fluctuated with overshooting the beach at a higher speed. Therefore, the corresponding study used a range of flow speeds showing a stable flow rate change while the closure area can be completely filled with air, and this limited range is also applied in this study as shown in Fig. 5. Similar experimental results can be found in other studies. More power was required to maintain the air cavity than not lubricating in some low-speed conditions, and if the flow is too low, the water might re-attach too close to the cavity step (Pavlov et al., 2020). In addition, according to Butterworth et al. (2015), the efficiency of the air cavity decreases as the speed increases. If it is too high, the bubbles may escape from the side of the cavity, resulting in negative net savings. However, the effect of reducing drag on the air layer and the leakage of air from the bottom of the hull is greatly influenced by the design characteristics of the bottom cavity (Slyozkin et al., 2014; Butterworth et al., 2015). If the air flow rate is optimized and the hull is properly designed for the PCDR, considering the ship's operating characteristics, the air lubrication system may also be functional in various speed ranges (Pavlov et al., 2020). From the review of previous work summarized in the preceding discussion, it might be concluded that air cavity is an immature type of ALS, requiring further research. However, we still chose to include it in this study.

To determine the amount of air required for each ALS, the model uses regression equations based on experimental data on the flat plate as shown in Eqs. (15)-(17). At sufficiently high Reynolds numbers, the dependence of gas flux on Reynolds number can be weakened (Lay et al., 2010), and in experiments with different size scales of comparable shape, the normalized gas flux for air lubrication may be in the same range (Makiharju et al., 2010; Mäkiharju et al., 2012). Thus, this study used the results of these model scales to estimate the actual gas flow rate on a full-scale ship. A curve fitting equation was developed based on the experimental results at the transition gas injection rate of BDR, and the gas flux necessary to accomplish ALDR and PCDR was then applied as demonstrated in the study of Mäkiharju et al. (2012). Here, the gas flux of ALDR was selected using the regression equation of the rough plate assuming that the surface of the hull would be somewhat rough rather than completely smooth. Instead of using the establishment gas flux of PCDR, maintenance was employed since it was assumed that keeping a cavity using an air lubricating system during the voyage would be more common. In this model, it is assumed that the air lubrication system is automatically controlled, such as the volume gas flux according to the flow speed shown in Fig. 5, and that the system automatically shuts off if the compressor consumes more power than the saving power or if it is outside the operating speed range.

The curve fits for volumetric air flux per unit span (q) for BDR at the transitional gas injection rate are as follows:

$$q_{BDR} = 0.008V - 0.0405 \quad 5.5 < V < 12.5 \tag{15}$$

The curve fits for volumetric air flux per unit span for ALDR on a rough surface, and the curve fits for maintaining PCDR are expressed:

$$q_{ALDR} = 0.00126V^2 - 0.00755V + 0.0391 \quad 5.5 < V < 12.5 \tag{16}$$

$$q_{PCDR} = 0.00701V^2 - 0.0866V + 0.277 \quad 5.5 < V < 7.5 \tag{17}$$

Table 2 shows the specifications and power of the compressor used for air lubrication systems reported in several studies. Here, main dimensions without accurate information from the references are obtained through a similar ship or simple estimation method (Kim et al., 2022a). By substituting the given information into Eqs. (10)-(13), the compressor powers of the various ships listed in the table are estimated, and they are compared in Fig. 6. As the operating conditions and information of the vessel and ALS compressor shown in the table do not exactly match the setting used in this model, it may be a rather rough estimate. However, as shown in the figure, estimates are quite well correlated with the reported data.

3.1.4. Weather correction for the efficiency of air lubrication system

Depending on the environment the vessel is operating in, the ALS performance may change. According to the sea-trial results for a cruise ship from Foreship (Pavlov et al., 2020), a relatively small

Table 2
Compressor specifications for air lubrication of ships from reported data. The asterisk symbol in the table represents the estimated value.

Ship type	L [m] × B [m] × T [m]	Speed [knots]	Air flow [m^3/min]	Compressor power [kW]	References
Bulk carrier	230 × 43 × 6.6–12.8	14	150–250	500–840	Mizokami et al. (2013)
Module carrier	153 × 38 × 4.5	13.25	40.5–94.5	72–211	Mizokami et al. (2010)
Tanker	168 × 32 × 10.6	11–14	–	150–230	Silberschmidt et al. (2016)
Container	350 × 51* × 15.5*	24	200–550	680–1900	Mizokami et al. (2013)
Container	321* × 45.6 × 14.75	19	133	600	Borusevich et al. (2017)
Ferry	105 × 17.9 × 6.3	14	26–110	13–60	Nagamatsu et al. (2002)
Passenger ship	240 × 32.2* × 7.8*	17	100–200	230–460	Mizokami et al. (2013)

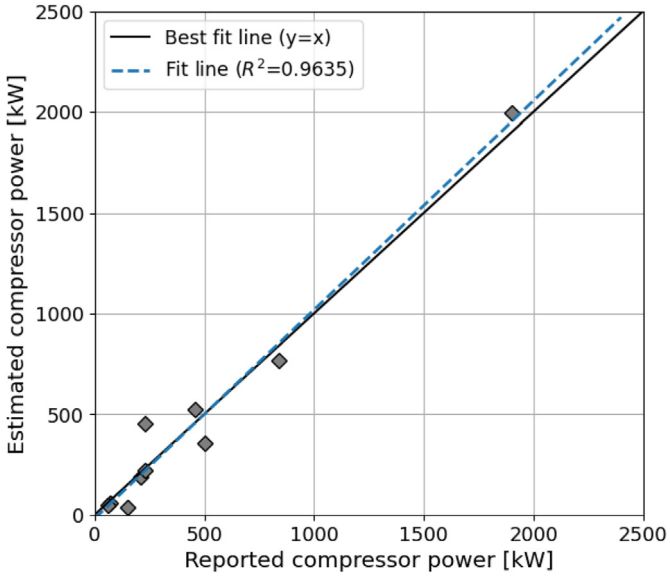

Fig. 6. Comparison of estimated compressor power from the model and the reported compressor power in Table 2.

tendency of net power saving due to air bubbles according to ALS on-off was seen for Beaufort scale 6 and above compared to less than Beaufort scale 4. According to the model test of a tanker by Borusevich et al. (2017), as the sea-state (ss) increased, cavity instability due to waves occurred in PCDR. As a result, the power saving efficiency of the air cavity system dropped by 20% in ss5, 40% in ss6, and 90% in ss7, and was hardly functional above. The extreme pitch motion of the ship in the rough sea is found to have the potential to seriously disturb the air layer on the bottom of the hull. As a result, the drag reduction from the air layer system is reduced, and more air is needed to keep the air lubrication at its calm water level.

It has been challenging to evaluate the effect of waves on the air lubrication system because the majority of ALS research has used model experiments in towing tanks or sea trials in relatively calm water conditions. As a result, this study used the findings of Borusevich et al. (2016) to roughly represent the effects of weather in the model. As indicated in Eq. (18), in order to estimate the power saving reflecting the weather effect, the power savings estimated by Eq. (4) is multiplied by the correction factor as shown in Table 3. Although it is cautiously expected that the air cavity system will have a greater loss due to ship motion than air bubble or air layer on the bottom surface, the coefficient is identically given to all ALS kinds and ship types. Nevertheless, further tests and full-scale observations are required to fully understand how weather affects ALS performance in relation to the sea state and ship design. A comparison of ALS performance according to the application of actual sea conditions and weather correction factors is further discussed in Section 4.4.

Table 3
Weather correction factor for the efficiency of air lubrication system according to the sea-state.

Sea-state	Max sig.wave height [m]	Correction factor [-]
1	0.1	1
2	0.5	1
3	1.25	1
4	2.5	1
5	4	0.8
6	6	0.6
7	9	0.1
8	–	0

$$P_{save,wc} = P_{save} \times C_{wc} \tag{18}$$

where $P_{save,wc}$ is saved power by air lubrication system after weather effect correction, C_{wc} is weather correction factor.

3.2. Comparison with previous studies

This section examines the validity of the model by comparing the results obtained from several experiments such as model tests, CFD, and full-scale measurements with the estimates of the model proposed in Section 3.1. Fig. 7(a) shows the results of CFD analysis for the 320 m cruise ship from Foreship (Pavlov et al., 2020). Here, the ship's speed changed from 14 knots to 22 knots, and net-percentage power savings for four different air flow rates were shown. According to CFD calculations, the power saved by air bubbles tends to drop constantly as ship speed increases at relatively low flow rates of 2.3–7.3 kg/s, however, at 10 kg/s, the saving rises until 19 knots and then declines. BDR estimations from the proposed model reflect a trend where savings gradually decrease as speed increases, while the ALDR estimates gradually grow with speed and then gradually fall beyond 18 knots. Although the figures do not exactly match, it seems to capture the saving trend of ALS according to the speed and flow rate of the ship. Compared to the CFD results, the volatility of net-percentage power saving with speed seems small, but comparing the model tests and full-scale measurements in Fig. 7(b), it can be seen that the volatility may not be so large.

The net-percentage power savings achieved by the air lubrication system during the laden voyage of a LNG ship are shown in Fig. 7(b). In the Model test, about 5–6% saving is attainable, and the optimal performance can be achieved near the ship's service speed, which is similar to the trend of ALDR predictions from the proposed model. In this experiment, two rows of air injectors in the forward and one in the aft were arranged at the bottom of the ship model, and the nominal thickness of the air layer was formed 2, 3, and 5 mm, respectively, which is presumed to correspond to transitional air layer drag reduction. The results show net-percentage power savings of roughly 4–5% from the ship's real operations, and they tend to decline slightly as speed increases, which is similar to the BDR predictions made by our model.

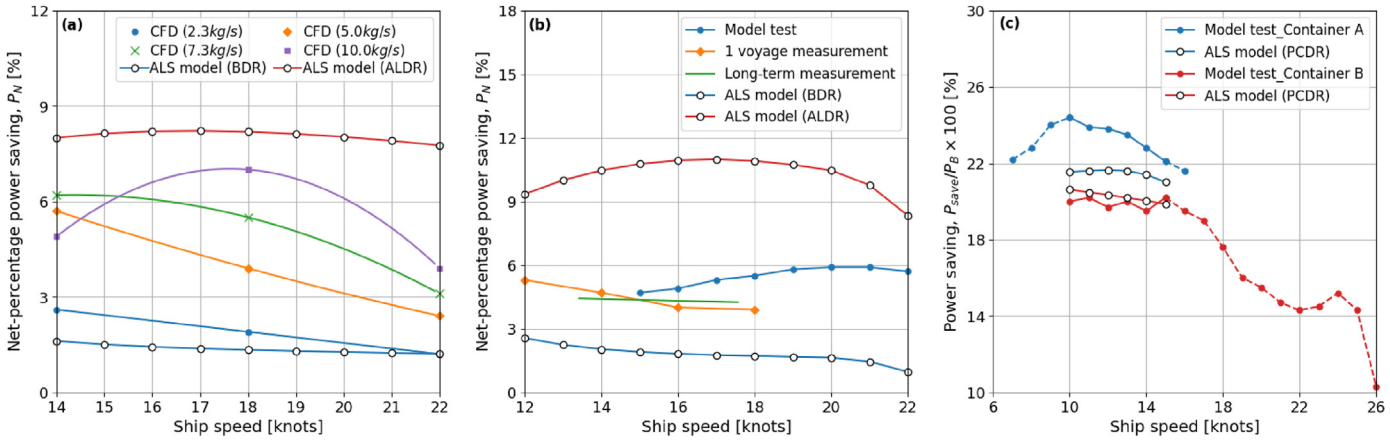

Fig. 7. Comparison of estimates of the proposed model with previous experimental results (a) Cruise ship (Pavlov et al., 2020), (b) LNG carrier (Lee et al., 2017), (c) Container ship A (Borusevich et al., 2017) and Container ship B (Pavlov et al., 2020). The figures are adapted from the referenced papers with minor modifications.

Fig. 7(c) shows the results of PCDR analysis of two container ships. As shown in the figure, it was not possible to collect the power consumption of the compressor according to speed from the relevant research (Borusevich et al., 2017; Pavlov et al., 2020), they were compared in terms of power saving by ALS, without correcting for compressor power. Looking at the predicted results, it can be seen that it is in quite good agreement with the results of two ships within the computable area.

The BDR estimates in this model tended to be somewhat smaller than the results of other studies, apparently because the BDR was calculated based on the transitional gas injection rate. Some of the studies related to the air bubble system may have progressed beyond the area where only air bubbles exist to the transitional region where air bubbles and air layers coexist through the adjustment of air flux. Overall, the ALDR has a tendency to overestimate, which is probably because this model assumes that a completely continuous air layer has been formed. In the case of PCDR, it tends to be almost similar to the experimental results within the application range. Fig. 7 shows that the prediction method presented in Section 3.1 gives fairly good estimates, seen in the light of the simplicity of the model and the complexity of the physics it attempts to represent. The comparison in Fig. 7 is also a reminder that our model is not intended to be an accurate representation and not a replacement for model tests or detailed numerical studies.

Due to the various assumptions and the settings of ALS in the model, these comparison results were not accurately matched. This model assumes that the air lubrication system is automatically controlled to maintain the drag reduction level at a specific air flow rate measured in the experiment. Moreover, an air layer is generated and maintained along the bottom of the hull without loss of bubbles, and the reduction in propulsive efficiency due to bubbles is ignored. In particular, during the actual operation of the ship, the drag reduction effect of the air layer may have been influenced by several uncertain factors such as the ship's motion, environments, and ship-specific conditions. As a result, it is difficult to replicate the precise conditions of tests undertaken in prior studies, hence this can only provide an approximation of the model's validity.

4. Results

4.1. Parametric study

The energy saving trend of the air lubrication technology was investigated using a parametric study on changes in ship speed, air covered area, loading condition, and block coefficients in accordance with various ship operating and design conditions. Here, a supramax-class general cargo ship was selected for the case study and had the dimensions shown in Table 4. The settings for each simulation case were specified as shown in Table 5, and the findings thereof are depicted in Fig. 8; the upper graph displays the net-percentage power saving, while the lower graph displays the net power saving. To investigate the influence of block coefficient in Case 4, it is assumed that the hull shape design has been modified, i.e., that the air lubrication system has been installed on different ships (85–100% C_b).

In Fig. 8(a), the net power saving increases for all ALS types as ship speed rises. While, the net-percentage power saving gradually declines in BDR, and for ALDR and PCDR, it is gradually increased to a certain speed and then decreased. In principle, it is advantageous for ships to operate at a low service speed because the frictional resistance is predominant at low speeds, while at high speeds, the wave-making resistance contributes more to the total resistance. However, since the air flux required by the compressor varies for each ALS type as illustrated in Fig. 5, the speed conditions at which the maximum saving could be achieved from the ALS could be slightly different.

The lower and upper limits of the net-percentage power saving are depicted in Fig. 8(b), which only changes the ratio of the air covered area from 60% to 100% under the same conditions as in Case 1. Due to the hull structure and arrangement of air release units, it is practically impossible to completely cover the bottom region with air; nonetheless, the range is assumed to be 60–100% to examine the effect of the air covered area. Depending on the ALS type, this difference in the air covered area may lead to a significant difference in savings of 3–10%. In other words, it is clear that the configurations of the ALS installation, which decide how much air can cover the bottom region, can have a significant impact on performance in addition to the ship's flat bottom area.

Table 4
Ship basic information.

	General cargo
Length [m]	194
Breadth [m]	32
Design draught [m]	12.6
Block coefficient [-]	0.79
Wetted surface area at design draught [m^2]	9370
Deadweight tonnage [ton]	50700
Maximum continuous rating [kW]	10780
Service speed [knots]	15.5

Table 5
Parametric study of the air lubrication systems for the target ship. Sea-states are assumed to be calm water condition.

Case	V_s [knots]	T [m]	C_b [-]	A_a/A_b [-]
1	10.5−15.5 (0.7−1.0V_s)	12.6	0.79	0.84
2	10.5−15.5 (0.7−1.0V_s)	12.6	0.79	0.6−1.0
3	15.5	8.8−12.6 (0.7−1.0T_d)	0.79	0.84
4	15.5	12.6	0.68−0.79 (0.85−1.0C_b)	0.84

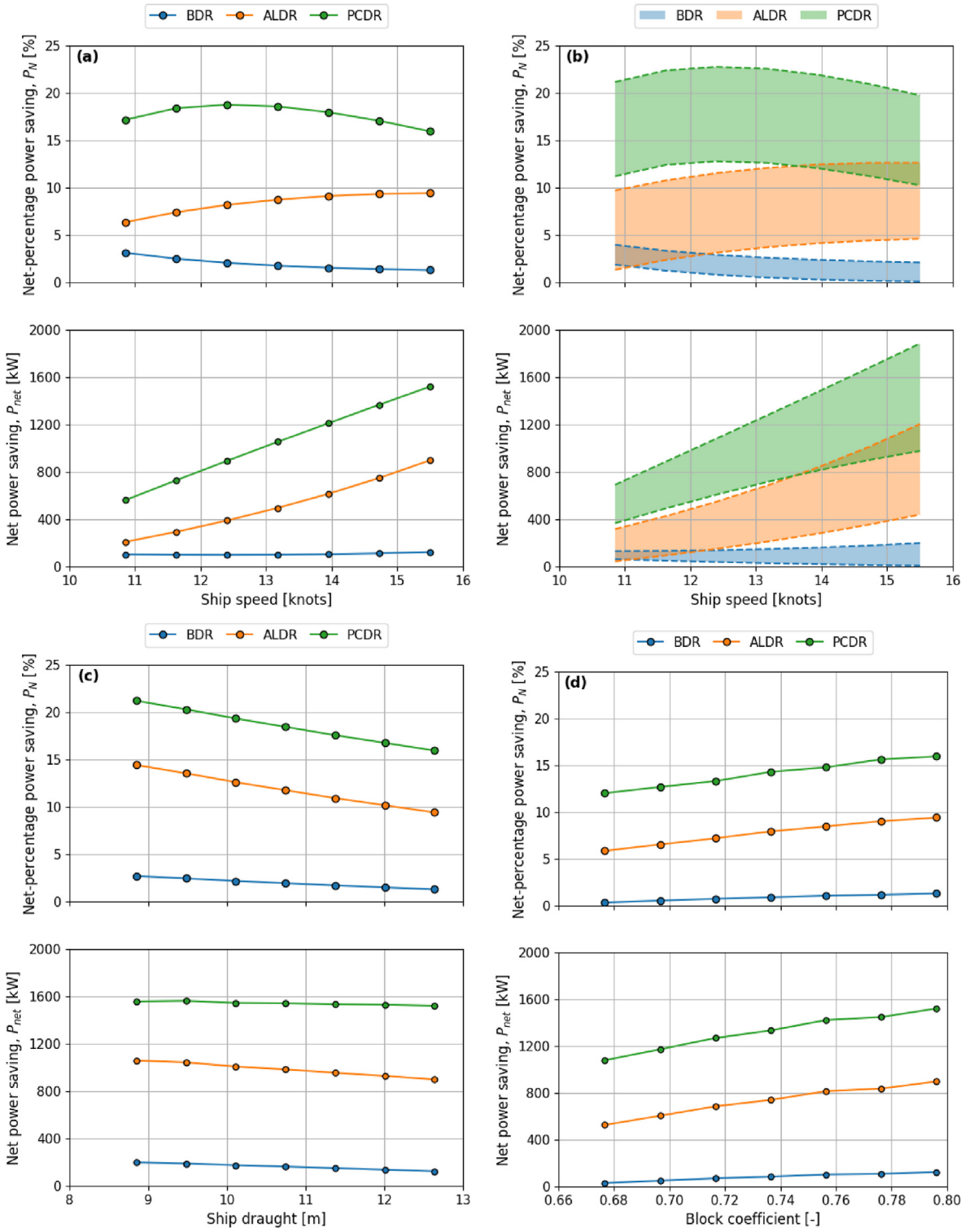

Fig. 8. Results of parametric study for the air lubrication systems: (a) speed, (b) ratio of air covered area to the bottom surface area, (c) draught, and (d) block coefficient.

Case 3 demonstrates that the net saving of the air lubrication decreases as the draught increases. This is because the energy consumed by the compressor to supply air to the bottom of the ship is increasing with increasing draught. Additionally, the underwater area increases along with the draught, increasing the hydrodynamic drag forces, which has the effect of increasing the overall required power.

Fig. 8(d) shows the parametric study results of the block coefficients. The bottom area of the ship generally tends to widen as the block coefficient increases, thus even if it is assumed that the same percentage of air is covering the hull bottom, it can be seen that the amount of frictional resistance can be decreased. That is, the efficiency of air lubrication system is high at a high block coefficient as can be observed from the figure.

4.2. Global sensitivity analysis

The Sobol method, a global sensitivity analysis method, was used to determine how each parameter affected the model's output. The Sobol sensitivity index can be used to quantify each parameter's contribution to the variance of the model output. A low Sobol index indicates that the variation of the output caused by a change in the corresponding parameter is relatively small (Homma and Saltelli, 1996; Saltelli and Annoni, 2010). The first-order index is measuring the direct effect of each parameter on the variance of the model. It can be expressed as Eq. (19), and it means an expected decrease in the variance of the model when X_i is fixed. The total index, which includes both the first-order index, as well as the sensitivity due to the interaction between that parameter and all other parameters, can be expressed as Eq. (20). The larger the difference between the first and total index, the greater the effect of sensitivity on variance due to the interaction.

$$S_i = \frac{Var[E(Y|X_i)]}{Var(Y)} \tag{19}$$

$$S_i^T = \frac{Var[E(Y|X_{-i})]}{Var(Y)} \tag{20}$$

where, $E(Y|X_i)$ stands for the predicted output value when X_i is fixed, and X_{-i} denotes all uncertain parameters except X_i.

Here, as shown in Fig. 9, global sensitivity was examined within the range (V_s: 10.5–15.5, T: 8.9–12.6, A_a/A_b: 0.6–1.0) that was taken into account in the previous section. Within this range, it was assumed that the parameters were distributed uniformly. For each sensitivity analysis group, different block coefficients were used of 0.68, 0.74, and 0.79 to support the assumption that the air lubrication system was installed on the different ships, respectively. As a result of the preliminary analysis, the interaction between speed, draught, and the ratio of air covered area to the bottom surface area was not significant, there was little difference between the total index and the first index. Thus, only the first-order Sobol indices are displayed in the figure. Within the parameter range defined in this research, the ratio of air covered area to the bottom surface area is the most influential as it accounts for about 46–85% of the total variance. In BDR, speed is a relatively more important parameter than ALDR and PCDR, which is about 35–42% of the total. The change in the Sobol index of various parameters according to block coefficient is not significant, but the influence of draught is relatively greater in ships with a large block coefficient.

4.3. Case study of global fleet in calm water condition

On about 48,710 global fleet registered in the Seaweb database, performance analysis in calm sea conditions according to the installation of the air lubrication system was carried out. Here, five ship categories of bulk carrier, chemical tanker, general cargo, container ship, and oil tanker were examined, and ship type and size were categorized in accordance with the IMO's fourth greenhouse gas study (IMO, 2020), as indicated in Table 6. The draught ratio for each ship type was used as given in Table 7 in order to assume the laden and ballast voyage of the ship operation (Olmer et al., 2017). Here, ballast-only voyages are uncommon for container ships unlike other ship types, thus the average draught ratio is applied for all voyage types. According to the study's specified bin size, Fig. 10 depicts the composition of each type of ship, and the distributions of ship parameters employed in this case study are shown in Fig. 11.

Fig. 12 displays the comparison of the global fleet's potential net-percentage power savings by type of air lubrication. The blue and red boxes represent the case study assuming that there is no environmental force when navigating at service speed under ballast and laden conditions.

The saving of the air lubrication system during a ballast voyage is higher than that of a laden voyage, as can be demonstrated in this plot. Container ships deliver the same results because their draught is assumed to be the same. Inspecting the overall results for each ship type, bulk carriers and tankers with flat bottom shapes that can hold more air bubbles in the hull bottom, i.e., generally associated with high block coefficients, are advantageous. Referring to Fig. 11, it can be seen that a ship with a relatively low operating speed compared to the size of the ship, that is, the Froude number, rather than the operating speed, has a more direct effect on power saving. The potential net-percentage power savings of BDR, ALDR, and PCDR are 2–5%, 8–14%, and 16–22%, respectively, when the results of the entire fleet of 25–75% quantile in ballast and laden

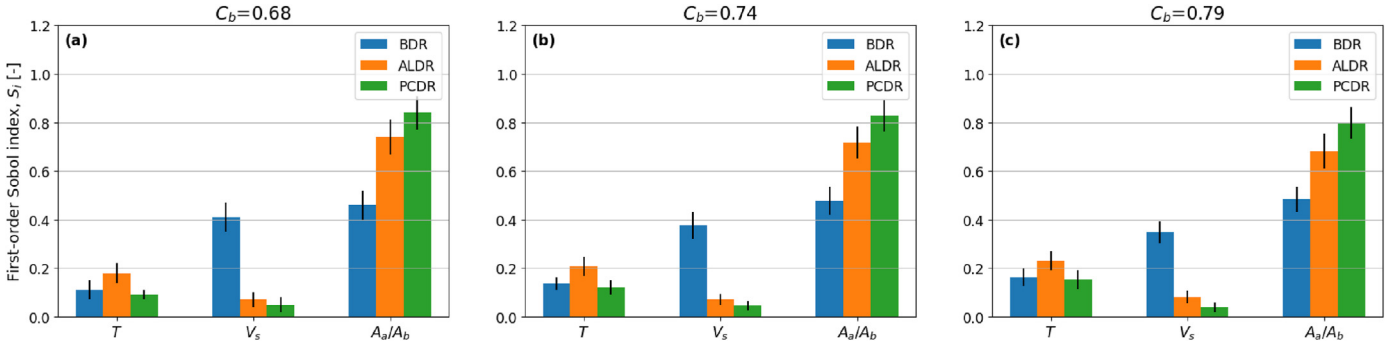

Fig. 9. Sensitivity analysis with Sobol's indices for each parameter according to different block coefficient. The bars in the figure represent the first order Sobol index using 10,000 random samples from the Monte Carlo method.

Table 6
Vessel type and categories.

Ship type	Bin size	Capacity	Unit
Bulk carrier	1	0-9999	DWT
	2	10,000–34,999	
	3	35,000–59,999	
	4	60,000–99,999	
	5	100,000–199,999	
	6	200,000-	
Chemical tanker	1	0-4999	DWT
	2	5000–9999	
	3	10,000–19,999	
	4	20,000–39,999	
	5	40,000-	
Container ship	1	0–999	TEU
	2	1000–1999	
	3	2000–2999	
	4	3000–4999	
	5	5000–7999	
	6	8000–11,999	
	7	12,000–14,999	
	8	14,500–19,999	
	9	20,000-	
General cargo	1	0-4999	DWT
	2	5000–9999	
	3	10,000–19,999	
	4	20,000–30,000	
Oil tanker	1	0-4999	DWT
	2	5000–9999	
	3	10,000–19,999	
	4	20,000–59,999	
	5	60,000–79,999	
	6	80,000–119,999	
	7	120,000–199,999	
	8	200,000-	

Table 7
Average draught ratio according to the voyage type of different ship types. Draught ratio is defined as the ratio of actual draught to design draught.

Ship type	Ballast voyage	Laden voyage
Bulk carrier	0.58	0.91
Chemical tanker	0.66	0.88
General cargo	0.65	0.89
Oil tanker	0.60	0.89
Container ship	0.82	

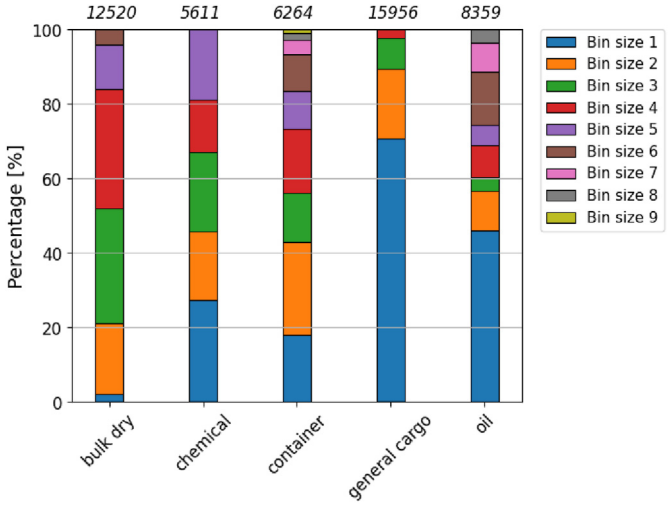

Fig. 10. Percentage of vessels by bin size obtained from the sea-web database.

voyages are taken into account.

A more detailed comparison according to the bin size for each ship type is displayed in the following Fig. 13. The PCDR results of some container ships are not provided here, which were not calculated because the service speeds of the vessels belonging to the corresponding bin sizes were outside the operating range of the PCDR. It is clear that even within the same ship type, performance can vary significantly depending on the operation profile and hull characteristics. Additionally, it can be shown that overall savings tend to rise as bin size grows. This is thought to be the case since the proportion of frictional resistance in total resistance increases with ship size. On the other hand, the net-percentage power savings tend to no longer increase but rather slightly decrease in the case of a large tanker such as bins 7 and 8 because the air compressor's power consumption rises due to the hull design with deep draught. Based on these results, coastal barges with flat bottom hull shapes that typically operate at low draught and low speeds are believed to be an ideal ship type, although not investigated in this study.

The results shown here are obtained under the assumption of calm water conditions and can be somewhat optimistic due to the various assumptions and simplifications. In order to obtain the corresponding amount of drag reduction on an actual ship, an appropriate design must follow. However, the estimated results in Fig. 12 are fairly consistent and are distributed in a similar range to the previous research as in Fig. 1, despite the fact that a ship-to-ship comparison between them cannot be done due to different experimental setups, such as ship speed, loading conditions, and air lubrication system.

Considering the actual use of air lubrication technology, the following characteristics can be considered from the above analysis results. For ships that are already in operation, the retrofit is comparatively easy with BDR and ALDR and a certain degree of drag reduction can be expected. Furthermore, it is investigated that the impact on the ship's maneuvering and sea-keeping capabilities is not significant (Thill et al., 2005; Foeth et al., 2009; Gallardo Martínez, 2016). However, according to the hull shape and operating profile, it is required to assess the actual gain between savings by air lubrication and consumption by the air compressor. Meanwhile, PCDR is expected to be effective when the ship maintains an air lubrication system throughout actual operations due to the relatively small air flux required to keep the air cavity. According to Zverkhovskyi and De Jong (2020), a recent tank test study on PCDR, it may be particularly suitable for hybrid and electric ships because it can significantly reduce energy consumption, helping to reduce the ship's capacity required for energy storage or power generation systems. However, initial capital costs may be high due to the need for a hull design specifically suited for PCDR. Additionally, the system can be functional in a limited range, and there is still some ambiguity regarding air cavity loss caused by ship motion. Furthermore, since most studies on PCDR are based on model experiments, further studies on a large scale are needed to determine effective and feasible operational range.

4.4. Case study of a target ship in real sea condition

In the previous section, due to a large amount of calculation of the global fleets, results were obtained by assuming calm water conditions, i.e., external environmental factors are ignored, but in this section, the performance of ALS according to the weather effect is analyzed. For ease of calculation, it is assumed that a ship operates a fixed trade pattern at service speed annually, and three different scenarios are compared: a calm sea condition, a real sea condition, and the real sea condition where weather adjustment factors are applied.

The general cargo ship in Table 4 was used, and a scenario was

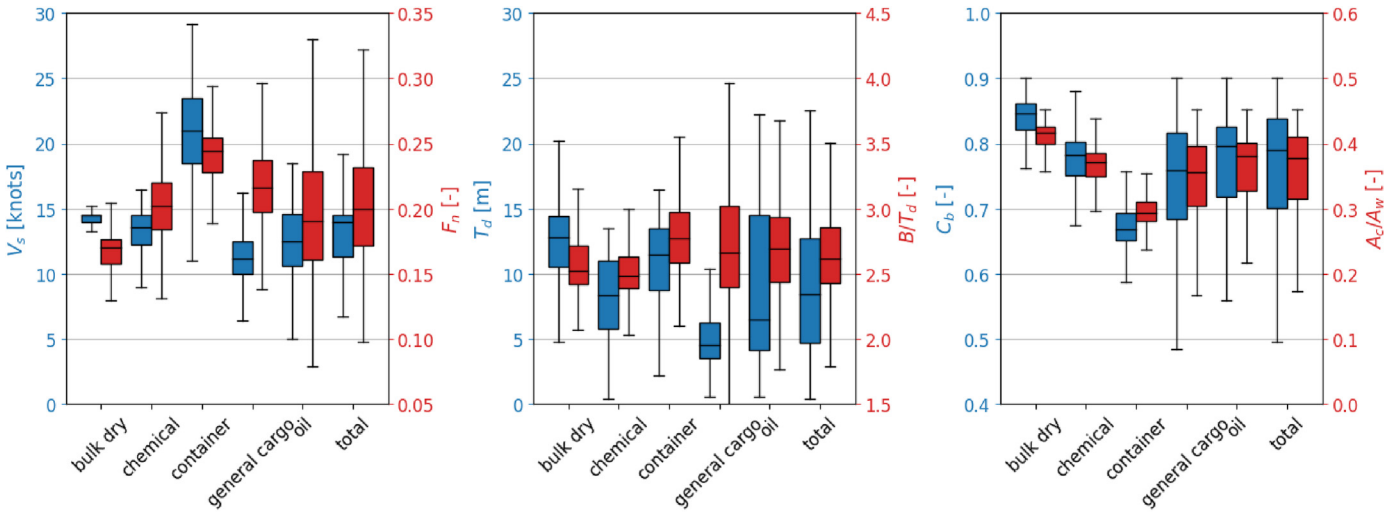

Fig. 11. Distribution of ship parameters relevant to ALS according to the ship type used in the study.

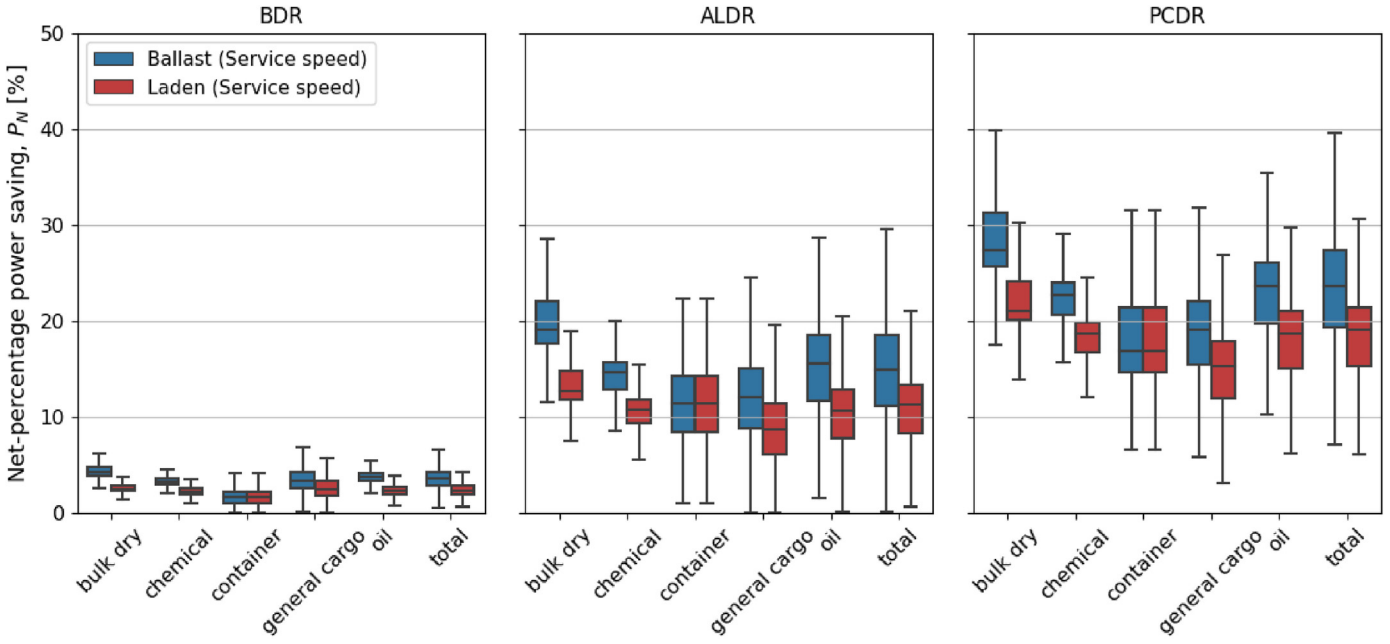

Fig. 12. Comparison of potential net power saving of global fleet by air lubrication type.

assumed in which the ship sailed the route between Rotterdam, Netherlands (NLRTM), and New York, USA (USNYC), at a constant service speed of 15.5 knots, as indicated in Fig. 14. NLRTM-USNYC is assumed as a laden voyage and in the opposite direction is ballast voyage, and 50 waypoints were uniformly defined throughout the route. The histograms of the apparent wind speed, apparent wind angle, significant wave height, and relative wave angle that the ship may experience while operating are presented in Fig. 15, which was created using meteorological data from the appropriate route from the ECMWF reanalysis weather hindcast data for 2020 (In the figure, 0° represents headwind and head wave). On average, the ship encounters more headwinds from NLRTM to USNYC and following winds from USNYC to NLRTM during the voyage.

Fig. 16 represents an example of ALDR in the ship's laden voyage among the results of annual energy-saving simulations, and Fig. 16(a) and Fig. 16(b) show seasonal changes and three different scenarios, respectively. The ship typically experiences headwinds at the start of the voyage outside the Strait of Gibraltar, and in the North Atlantic Ocean, net-percentage power savings tend to decline dramatically as a result of rather strong external environments, since the total resistance increases significantly, while the frictional resistance reduction by ALS is not influenced. In addition, seasonal variations show that from June to August, there is an average saving of about 8%, while from December to February, the average saving in some areas drops to less than 4%. It is evident that there is a significant variation in the performance efficiency of air lubrication depending on the region and season. In Fig. 16(b), the difference in net-percentage power saving according to the actual weather conditions at sea can be confirmed. In calm sea conditions, the savings of the ship is constant annually at all waypoints, but when considering the weather profiles of the real sea, the net-percentage power saving changes geographically and seasonally, and there is a

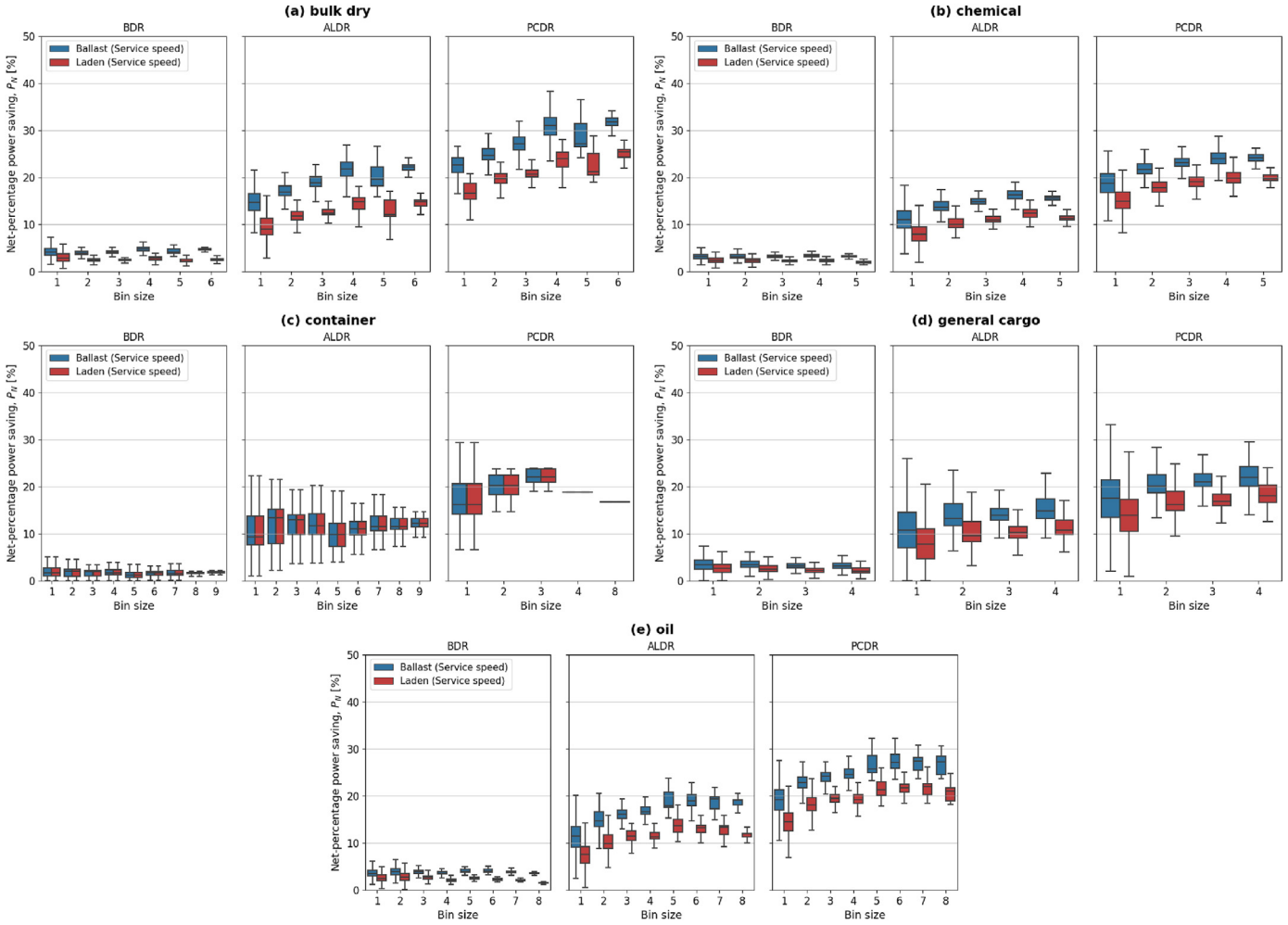

Fig. 13. Comparison of potential net power saving of global fleet in bin categories according to ship type: (a) bulk dry, (b): chemical, (c): container, (d): general cargo, (e) oil.

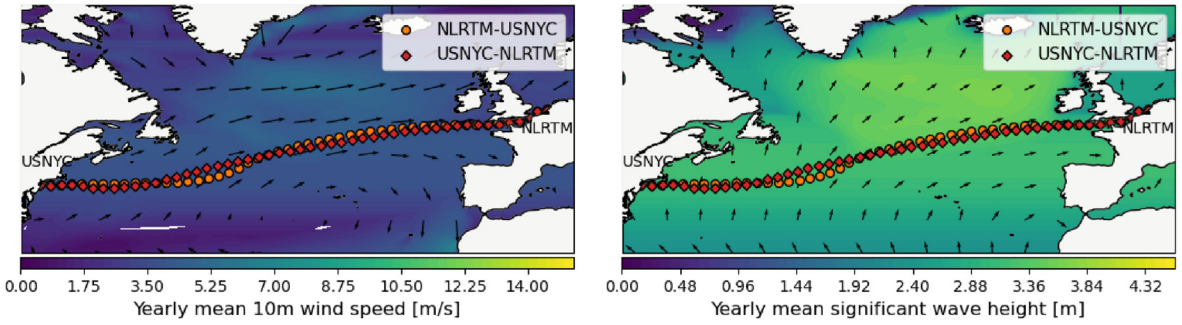

Fig. 14. (a) Yearly mean wind speed, (b) Yearly mean significant wave height at North Atlantic Ocean in 2020. Arrows in the figures represent the mean direction of the wind and waves. Orange circle is route from NLRTM to USNYC and red diamond is from USNYC to NLRTM.

difference of about 30% on average. When the weather adjustment factor proposed in this study is additionally applied, it tends to decrease by about 5% more than that. Thus, the weather correction factor itself is of minor importance compared to the increase of resistance and related power consumption due to wind and waves. Fig. 17 shows the results of three scenarios for all ALS types and voyage types at once. It can be seen that the overall energy-saving effect decreases by roughly 15–35% compared to the calm water conditions, taking into account the actual weather environment and weather correction effect. The difference in efficiency between the ballast voyage and the laden voyage is also shown in Fig. 17, which is expected to be largely due to the meteorological characteristics of such a specified route, where the annual weather condition is much more severe in the laden voyage, as shown Fig. 15.

5. Conclusions

Most of the existing studies related to ALS have introduced ship-specific approaches such as model tests, CFD, and full-scale measurements, and few simplified models can be applied to various

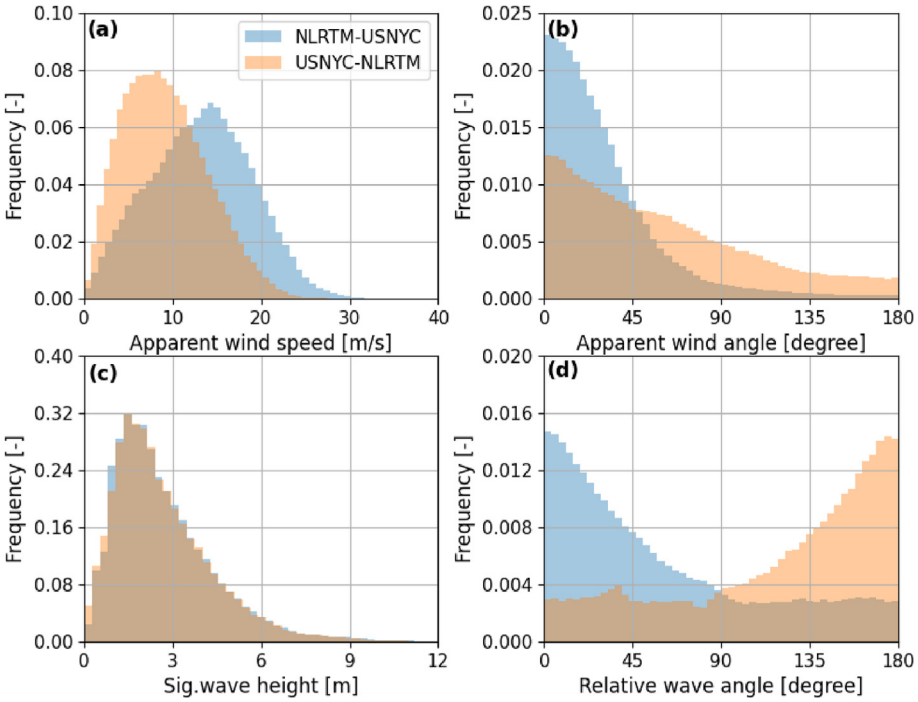

Fig. 15. Histograms of the actual weather conditions that ship encounters: (a) apparent wind speed, (b) apparent wind angle, (c) significant wave height, (d) relative wave angle.

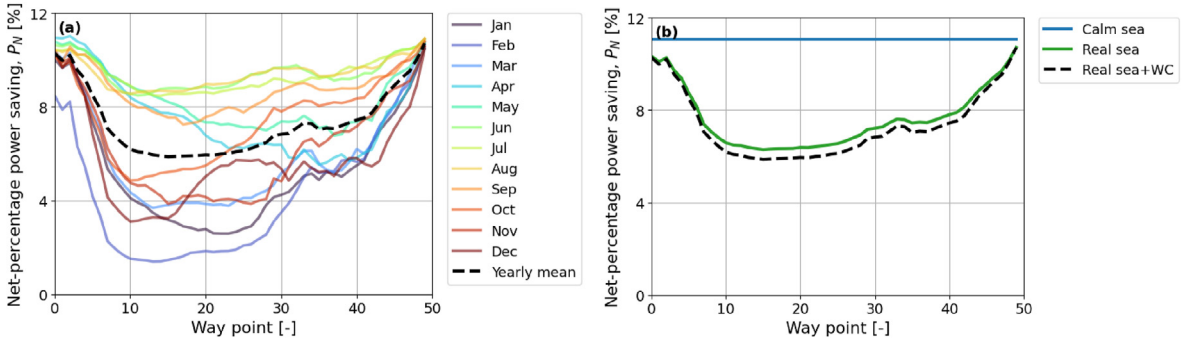

Fig. 16. Net power savings of a ship using ALDR at laden voyage (NLRTM-USNYC): (a) seasonal changes, (b) weather influences.

vessels with different operating profiles and evaluate energy-saving trends. This study presents an easy-to-use tool that can be applied at the global fleet level in order to assess the energy saving potential of air lubrication systems of different configurations. The tool might also be useful for early-design considerations of installation of air lubrication systems. The overall theoretical background underpinning the modeling, the estimation methods of several factors, and the assumptions were addressed. On the basis of the established model, parametric and sensitivity analyses were carried out, and insights on the variables influencing ALS performance were provided. Additionally, potential energy reduction trends for each ship type were examined, and changes in performance according to the location and seasonal effects were discovered for specific waters.

Through the parametric study, despite air lubrication systems being more efficient for ships operating at low speeds, the parametric study indicates that the ideal operating conditions may vary slightly depending on the type of air lubrication. The efficiency of ALS increases as the block coefficient rises because high block usually comes with large flat bottom area. Not only this, but it is also important how much air can cover the bottom area of the ship in relation to the configuration of ALS. The ratio of air covered area to the bottom surface area could explain 46–85% of the total variation of net-percentage power savings within the given parameter range in this study, according to a sensitivity analysis utilizing the Sobol index. As higher draught increases the energy needed to overcome hydrodynamic drag forces and increases the energy of the compressor used to supply air, the savings are larger in ballast than in laden conditions.

According to the case study conducted under the assumption that the entire global fleet would be equipped with ALS, the possible net-percentage power savings would be BDRs of 2–5%, ALDRs of 8–14%, and PCDRs of 16–22%. The level of savings identified in the fleet-wide study agrees fairly well with the level of savings of the various studies of individual ships found in the literature. Overall, bulk carriers and tanker with blunt hulls and moderate running speeds showed larger savings than container ships with slender hulls and high operating speeds. The operation profile and hull features, however, can significantly affect performance even within the same ship class. Considering the actual weather environment and weather correction effect, it can be

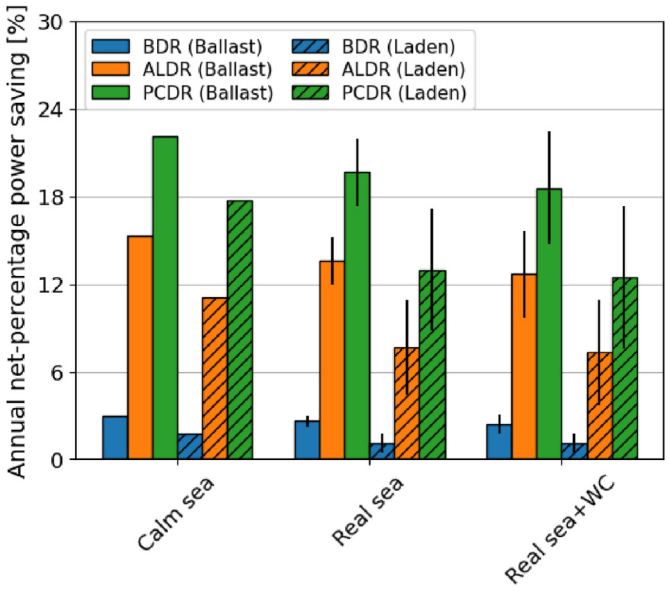

Fig. 17. Comparison of average annual net power saving of ALS according to the application of weather effects.

observed that the effect decreases by about 15–35% compared to the calm water conditions.

The approach taken in this study can be applied to provide preliminary performance estimates when considering the installation of an air lubricating system during the ship's initial design phase, and an evaluation of the anticipated performance of the global fleet can also be taken into consideration. In the area of international shipping, this will help to emphasize the potential of air lubrication technology to reduce emissions.

Nonetheless, it should be noted that some of the assumptions and simplifications of the model might lead to somewhat optimistic results. In fact, careful hull and system design suited to those systems will be needed to achieve the same level of power reduction as the results achieved from this work. The model would benefit from an improved model of the effect of waves and ship motions on the ALS, as well as the effect of ALS on the propulsive efficiency. Further study of airflow at large scales and high Reynolds numbers, as well as closer examination using full-scale measurements from ALS-equipped ships, are necessary in order to close the gap between model-scale and full-scale results and to more accurately capture the impact of the air layer below the hull. In addition, BDR and ALDR can be interconverted depending on the gas flow rate, and theoretically, there is an optimal gas flow rate that can provide maximum energy savings. This may vary depending on the design characteristics and operational profile of the vessel and need be constantly controlled during actual ALS operation. In a future study, it is planned to analyze the energy saving and related emission reduction potential from the optimized operation of air lubrication, taking into account the actual operational pattern and environment, including the wave correction on the air lubrication effectiveness.

Declaration of competing interest

The authors declare that they have no known competing financial interests or personal relationships that could have appeared to influence the work reported in this paper.

Acknowledgements

This study is part of the research projects CLIMMS – Climate change mitigation in the maritime sector (Research Council of Norway (RCN) project number 294771).

Appendix A

Table A.1
Relevant studies on the energy saving of air lubrication systems used in Fig. 1.

Type of ALS	Method	References
BDR	Model test	Kodama et al. (2005); Lee et al. (2017)
	Sea-trial	Latorre et al. (2002); Nagamatsu et al. (2002); Hoang et al. (2009); Kumagai et al. (2015); Silberschmidt et al. (2016); Lee et al. (2017); Mizokami and Kuroiwa (2019); Pavlov et al. (2020); Silverstream (2022)
	CFD	Pavlov et al. (2020)
ALDR	Model test	Jang et al. (2014); Lee et al. (2017); Sindagi et al. (2022)
	Sea-trial	Kodama et al. (2008); Hoang et al. (2009); Mizokami et al. (2010); Lee et al. (2017); Pavlov et al. (2020)
	CFD	Fotopoulos and Margaris (2020)
PCDR	Model test	Butterworth et al. (2015); Borusevich et al. (2016); Borusevich et al. (2017); Pavlov et al. (2020)
	Sea-trial	Aronietis et al. (2011); Borusevich et al. (2016); Pavlov et al. (2020)

Table A.2
Dimension of ships used for the regression equations in Eq. (9)

Ship type	L_{pp} [m]	B [m]	T_d [m]	C_b [-]	References
Tanker	161–323	28–60	9–21	0.72–0.85	Pinkster (1980); Bunnik (1999); Larsson et al. (2013); Park et al. (2019a); Hinostroza et al. (2019); Kim et al. (2019)
General cargo	60–194	15–32	3.2–12.6	0.56–0.80	Gupta et al. (2019); Gerritsma and Beukelman (1972); Kracht (1984); Alamsyah et al. (2018)
Bulk carrier	192	36	11.2	0.85	Lee et al. (2019)
Container	119–355	19–51	6–14.5	0.58–0.76	El-Moctar et al. (2012); Van (1997); Simonsen et al. (2013); Park et al. (2019b); Reguram et al. (2016); Liu et al. (2015)
Ro-Ro/Ferry	158–178	21–32	6.1–8.2	0.54–0.56	Tsujimoto et al. (2009); Surendran et al. (2005)
Total	60–355	15–60	3.2–21	0.55–0.85	

References

ABS, 2019. Air Lubrication Technology. American Bureau of Shipping, Spring, TX, USA.

Alamsyah, M.A., Hakim, M.L., Utama, I., 2018. Study of shear and pressure flow on the variation of ship hull shapes as one of the biofouling growth factors. In: Proceedings of the 3rd International Conference on Marine Technology. SCITEPRESS-Science and Technology Publications, pp. 97–105.

Aronietis, R., Crozet, Y., Ferrari, C., Frouws, K., Grootbod, H., Guihery, L., Kapros, S., Laroche, F., Lloyd, M., Rouboumtsos, A., et al., 2011. Innosutra Project Deliverable D4 and D5-Topical Assessment of Innovative Successes and Not-Yet-Successes.

Birk, L., 2019. Fundamentals of Ship Hydrodynamics: Fluid Mechanics, Ship Resistance and Propulsion. John Wiley & Sons.

Blendermann, W., 1996. Wind Loading of Ships Collected Data from Wind Tests Tunnel in Uniform Flow. Institut fur Schiffbau der Universitat Hamburg.

Borusevich, V., Poustoshny, A., Sverchkov, A., Trincas, G., 2017. Future Outlook of Artificial Cavity Application for Reducing Hydrodynamic Resistance of Containerships.

Borusevich, V., Pustoshny, A., Sverchkov, A., Trincas, G., 2016. Impact of air cavity technology on ship drag reduction: experience from research studies. In: 10th Symposium on High-Performance Marine Vehicles-HIPER 16. TUHH, pp. 94–107.

Bouman, E.A., Lindstad, E., Rialland, A.I., Strømman, A.H., 2017. State-of-the-art technologies, measures, and potential for reducing ghg emissions from shipping–a review. Transport. Res. Transport Environ. 52, 408–421.

Buckingham, J., Pearson, D., 2019. Modelling Alternative Propulsion Technologies for Merchant Vessels. RINA, Power & Propulsion Alternatives for Ships, 23rd January.

Bunnik, T.H., 1999. Seakeeping Calculations for Ships, Taking into Account the Nonlinear Steady Waves.

Butterworth, J., Atlar, M., Shi, W., 2015. Experimental analysis of an air cavity concept applied on a ship hull to improve the hull resistance. Ocean. Eng. 110, 2–10.

Ceccio, S.L., 2010. Friction drag reduction of external flows with bubble and gas injection. Annu. Rev. Fluid Mech. 42, 183–203.

Ceccio, S.L., Mäkiharju, S., 2012. Air Lubrication Drag Reduction on Great Lakes Ships. Great Lakes Maritime Research Institute.

Comer, B., Chen, C., Stolz, D., Rutherford, D., 2019. Rotors and bubbles: route-based assessment of innovative technologies to reduce ship fuel consumption and emissions. J. ICCT working pa per 11, 6.

Elbing, B.R., Mäkiharju, S., Wiggins, A., Perlin, M., Dowling, D.R., Ceccio, S.L., 2013. On the scaling of air layer drag reduction. J. Fluid Mech. 717, 484–513.

Elbing, B.R., Winkel, E.S., Lay, K.A., Ceccio, S.L., Dowling, D.R., Perlin, M., 2008. Bubble-induced skin-friction drag reduction and the abrupt transition to air-layer drag reduction. J. Fluid Mech. 612, 201–236.

El-Moctar, O., Shigunov, V., Zorn, T., 2012. Duisburg test case: post-panamax container ship for benchmarking. Ship Technol. Res. 59, 50–64.

Foeth, E., Eggers, R., van der Hout, I., Quadvlieg, F., 2009. Reduction of Frictional Resistance by Air Bubble Lubrication. SNAME Maritime Convention, OnePetro.

Fotopoulos, A.G., Margaris, D.P., 2020. Computational analysis of air lubrication system for commercial shipping and impacts on fuel consumption. Computation 8, 38.

Fujiwara, T., 2006. A new estimation method of wind forces and moments acting on ships on the basis of physical components models. J. Jpn. Soc. Nav. Archit. Ocean Eng. 2, 243–255.

Gallardo Martínez, A., 2016. Investigation of the Air-Lubrication Effect on Friction Resistance.

Gebraad, J., Quispel, M., Karaarslan, S., Lehne, M., Rafael, R., Eppich, M., Janssens, G., Smidt, H., Barcanescu, M., 2021. Structuring towards zero emission waterborne transport, d2.1. state-of-play of decarbonisation of waterborne transport "technology application atlas. https://www.waterborne.eu/projects/coordination-projects/steerer/results.

Gerritsma, J., Beukelman, W., 1972. Analysis of the resistance increase in waves of a fast cargo ship. Int. Shipbuild. Prog. 19, 285–293.

Guldhammer, H., Harvald, S.A., 1974. Ship resistance-effect of form and principal dimensions.(revised). In: Danmark, Danmarks Tekniske Hojskole, Kademisk Forlag, vol. 8. Danish Technical Press, St. kannikestrade. DK 1169 Copenhagen.

Gupta, P., Steen, S., Rasheed, A., 2019. Big data analytics as a tool to monitor hydrodynamic performance of a ship. In: International Conference on Offshore Mechanics and Arctic Engineering. American Society of Mechanical Engineers. V07AT06A059.

Helmore, P., 2008. Update on van oortmerssen's resistance prediction. In: Pacific 2008 International Maritime Conference.

Hinostroza, M., Xu, H., Soares, C.G., 2019. Manoeuvring test for a self-running ship model in various water depth conditions. In: Sustainable Development and Innovations in Marine Technologies. CRC Press, pp. 187–196.

Hoang, C., Toda, Y., Sanada, Y., 2009. Full scale experiment for frictional resistance reduction using air lubrication method. In: The Nineteenth International Offshore and Polar Engineering Conference. OnePetro.

Hollenbach, K.U., 1998. Estimating resistance and propulsion for single-screw and twin-screw ships-ship technology research 45 (1998). Schiffstechnik 45, 72.

Holtrop, J., Mennen, G., 1982. An approximate power prediction method. Int. Shipbuild. Prog. 29, 166–170.

Homma, T., Saltelli, A., 1996. Importance measures in global sensitivity analysis of nonlinear models. Reliab. Eng. Syst. Saf. 52, 1–17.

IMO, 2018. Strategy on reduction of ghg emissions from ships. MEPC 304, 72.

IMO, 2020. Fourth imo ghg study: reduction of ghg emissions from ships. MEPC 75, 7–15.

IMO, 2021. G. uidelines on the method of calculation of the attained energy efficiency existing ship index (eexi). MEPC 76/15/Add.2/Annex 7.

ISO, E., 2015. Sistema de Gestão da Qualidade, 9001: 2015.

ITTC, 1978. Report of performance committee. In: Proceedings 15th ITTC, pp. 389–392.

Jang, J., Choi, S.H., Ahn, S.M., Kim, B., Seo, J.S., 2014. Experimental investigation of frictional resistance reduction with air layer on the hull bottom of a ship. Int. J. Nav. Archit. Ocean Eng. 6, 363–379.

Kawabuchi, M., Kawakita, C., Mizokami, S., Higasa, S., Kodan, Y., Takano, S., 2011. Cfd predictions of bubbly flow around an energy-saving ship with mitsubishi air lubrication system. Mitsubishi Heavy Industries Technical Review 48, 53–57.

Kawakita, C., Takano, S., Kodan, Y., Mizokam, S., 2011. Experimental investigation of the behavior of injected air on the ship bottom and its influence on propeller. J. Jpn. Soc. Nav. Archit. Ocean Eng. 12, 43–50.

Kawashima, H., Kodama, Y., Hinatsu, M., Hori, T., Makino, M., Ohnawa, M., Takeshi, H., Sakoda, M., Kawashima, H., Matsuno, F., 2007. A research project on application of air bubble injection to a full scale ship for drag reduction. In: Fluids Engineering Division Summer Meeting, pp. 265–274.

Kim, H.T., Kim, H.T., Kim, H.J., Kim, J.J., 2021. Study on the evaluation of frictional drag reduction by air lubrication and the arrangement of air injection parts for a liquefied natural gas carrier. Journal of the Society of Naval Architects of Korea 58, 144–157.

Kim, T., Yoo, S., Oh, S., Kim, H.J., Lee, D., Kim, B., 2019. Numerical and experimental study on the estimation of added resistance of an lng carrier in waves. Int. J. Offshore Polar Eng. 29, 24–32.

Kim, Y., Steen, S., Muri, H., 2022a. A novel method for estimating missing values in ship principal data. Ocean. Eng. 251, 110979.

Kim, Y.R., Esmailian, E., Steen, S., 2022b. A meta-model for added resistance in waves. Ocean. Eng. 266, 112749.

Kodama, Y., Takahashi, T., Makino, M., Hori, T., Ueda, T., Kawamura, N., Shibata, M., Kato, H., Inoue, T., Suzuki, T., et al., 2005. Practical application of microbubbles to ships—large scale model experiments and a new full scale experiment. In: Proceedings of the 6th International Symposium on Smart Control of Turbulence.

Kodama, Y., Hinatsu, M., Hori, T., Kawashima, H., Takeshi, H., Makino, M., Ohnawa, M., Sanada, Y., Murai, Y., Ohta, S., 2008. A full-scale air lubrication experiment using a large cement carrier for energy saving (result and analysis). In: Proc. Japan Soc. Naval Architects and Ocean Engineers Conference, pp. 163–166.

Kracht, A., 1984. Einfluss des Bugwulstes auf den Leistungsbedarf eines Schiffes im Seegang. Forschungszentrum des Dt. Schiffbaus.

Kramel, D., Muri, H., Kim, Y., Lonka, R., Nielsen, J.B., Ringvold, A.L., Bouman, E.A., Steen, S., Strømman, A.H., 2021. Global shipping emissions from a well-to-wake perspective: the mariteam model. Environ. Sci. Technol. 55, 15040–15050.

Kristensen, H.O., Lützen, M., 2012. Prediction of resistance and propulsion power of ships. Clean Shipping Currents 1, 1–52.

Kumagai, I., Takahashi, Y., Murai, Y., 2015. Power-saving device for air bubble generation using a hydrofoil to reduce ship drag: theory, experiments, and application to ships. Ocean. Eng. 95, 183–194.

Larsson, L., Stern, F., Visonneau, M., 2013. Cfd in ship hydrodynamics—results of the gothenburg 2010 workshop. In: MARINE 2011, IV International Conference on Computational Methods in Marine Engineering. Springer, pp. 237–259.

Latorre, R., Miller, A., Philips, R., 2002. Microbubble resistance reduction for high-speed craft. SNAME Transactions 110, 259–277.

Lay, K.A., Yakushiji, R., Makiharju, S., Perlin, M., Ceccio, S.L., 2010. Partial cavity drag reduction at high Reynolds numbers. J. Ship Res. 54, 109–119.

Lee, C.M., Yu, J.W., Choi, J.E., Lee, I., 2019. Effect of bow hull forms on the resistance performance in calm water and waves for 66k dwt bulk carrier. Int. J. Nav. Archit. Ocean Eng. 11, 723–735.

Lee, J., Kim, J., Jang, J., McStay, P., Raptakis, G., Fitzpatrick, P., 2017. Full Scale Applications of Air Lubrication for Reduction of Ship Frictional Resistance. SNAME Maritime Convention, OnePetro.

Liu, W., Suzuki, K., Shibanuma, K., 2015. Nonlinear dynamic response and structural evaluation of container ship in large freak waves. J. Offshore Mech. Arctic Eng. 137.

Mäkiharju, S., Ceccio, S.L., 2011. Air Lubrication Drag Reduction on Great Lakes Ships. University of Michigan.

Makiharju, S., Elbing, B., Wiggins, A., Dowling, D., Perlin, M., Ceccio, S., 2010. Perturbed partial cavity drag reduction at high Reynolds numbers. In: Proc. 28th Symp. On Naval Hydrodynamics.

Mäkiharju, S.A., Elbing, B.R., Wiggins, A., Schinasi, S., Vanden-Broeck, J.M., Perlin, M., Dowling, D.R., Ceccio, S.L., 2013. On the scaling of air entrainment from a ventilated partial cavity. J. Fluid Mech. 732, 47–76.

Mäkiharju, S.A., Perlin, M., Ceccio, S.L., 2012. On the energy economics of air lubrication drag reduction. Int. J. Nav. Archit. Ocean Eng. 4, 412–422.

Mizokami, S., Kawakado, M., Kawano, M., Hasegawa, T., Hirakawa, I., 2013. Implementation of ship energy-saving operations with mitsubishi air lubrication system. Mitsubishi Heavy Industries Technical Review 50, 44–49.

Mizokami, S., Kawakita, C., Kodan, Y., Takano, S., Higasa, S., Shigenaga, R., 2010. Experimental study of air lubrication method and verification of effects on actual hull by means of sea trial. Mitsubishi Heavy Industries Technical Review

47, 41–47.
Mizokami, S., Kuroiwa, R., 2019. Installation of Air Lubrication System for Ro-Pax Ferry and Verification of its Effect in Actual Seas Based on Onboard Measurement Data, vol. 29. Japan Society of Naval Architects and Ocean Engineers, pp. 1–9.
Nag, P., 2013. Engineering Thermodynamics. Tata McGraw-Hill Education.
Nagamatsu, T., Kodama, Y., Kakugawa, A., Takai, M., Murakami, K., Ishikawa, S., Kamiirisa, H., Ogiwara, S., Yoshida, Y., Suzuki, T., et al., 2002. A full-scale experiment on microbubbles for skin friction reduction using" seiun maru" part 2: the full-scale experiment. J. Soc. Nav. Archit. Jpn. 15–28, 2002.
Olmer, N., Comer, B., Roy, B., Mao, X., Rutherford, D., 2017. Greenhouse Gas Emissions from Global Shipping, 2013–2015 Detailed Methodology. International Council on Clean Transportation, Washington, DC, USA, pp. 1–38.
Park, D.M., Lee, J.H., Jung, Y.W., Lee, J., Kim, Y., Gerhardt, F., 2019a. Experimental and numerical studies on added resistance of ship in oblique sea conditions. Ocean. Eng. 186, 106070.
Park, D.M., Lee, J.H., Lee, J., Kim, B.S., Kim, B.S., Yang, K.K., Kim, Y., Lee, Y.G., Kim, T., Yang, J.H., et al., 2019b. Comparative study on added resistance of a container ship in waves. In: The 29th International Ocean and Polar Engineering Conference. OnePetro.
Oosterveld, M.W.C., Van Oossanen, P., 1975. Further computer-analyzed data of the wageningen b-screw series. Int. Shipbuild. Prog. 22, 251–262.
Park, S.H., Lee, I., 2018. Optimization of drag reduction effect of air lubrication for a tanker model. Int. J. Nav. Archit. Ocean Eng. 10, 427–438.
Pavlov, G.A., Yun, L., Bliault, A., He, S.L., 2020. Air Lubricated and Air Cavity Ships. Springer.
Pinkster, J.A., 1980. Low Frequency Second Order Wave Exciting Forces on Floating Structures.
Reguram, B.R., Surendran, S., Lee, S.K., 2016. Application of fin system to reduce pitch motion. Int. J. Nav. Archit. Ocean Eng. 8, 409–421.
Saltelli, A., Annoni, P., 2010. How to avoid a perfunctory sensitivity analysis. Environ. Model. Software 25, 1508–1517.
Silberschmidt, N., Tasker, D., Pappas, T., Johannesson, J., 2016. Silverstream system-air lubrication performance verification and design development. In: Conference of Shipping in Changing Climate, pp. 10–11. Newcastle, UK.
Silverstream, 2022. Silverstream® system performance. URL: https://www.silverstream-tech.com/what-is-air-lubrication/.
Simonsen, C.D., Otzen, J.F., Joncquez, S., Stern, F., 2013. Efd and cfd for kcs heaving and pitching in regular head waves. J. Mar. Sci. Technol. 18, 435–459.
Sindagi, S., Vijayakumar, R., Saxena, B.K., 2022. Experimental investigation on ship's model in carrying out energy economics of bdr/als methodology. Ships Offshore Struct. 17, 1437–1446.
Slyozkin, A., Atlar, M., Sampson, R., Seo, K.C., 2014. An experimental investigation into the hydrodynamic drag reduction of a flat plate using air-fed cavities. Ocean Eng. 76, 105–120.
Surendran, S., Lee, S., Reddy, J.V.R., Lee, G., 2005. Non-linear roll dynamics of a ro-ro ship in waves. Ocean. Eng. 32, 1818–1828.
Thill, C., Toxopeus, S., van Walree, F., 2005. Project energy-saving air-lubricated ships (pels). In: Proceedings of the 2nd International Symposium on Seawater Drag Reduction, pp. 1–16.
Tsujimoto, M., Kuroda, M., Shibata, K., Sogihara, N., Takagi, K., 2009. On a calculation of decrease of ship speed in actual seas. J. Jpn. Soc. Nav. Archit. Ocean Eng. 9, 79–85.
Van, S., 1997. Measurement of flows around a 3600teu container ship model. In: Annual Autumn Meeting. SNAK, Seoul, Korea, 1997.
Van Oortmerssen, G., 1971. A power prediction method and its application to small ships. ISP 18.
Verschoof, R.A., Van Der Veen, R.C., Sun, C., Lohse, D., 2016. Bubble drag reduction requires large bubbles. Phys. Rev. Lett. 117, 104502.
Wu, H., Ou, Y.p., 2019. Experimental study of air layer drag reduction with bottom cavity for a bulk carrier ship model. China Ocean Eng. 33, 554–562.
Zhang, X., Bao, Z., Ge, Y.E., 2021. Investigating the determinants of shipowners' emission abatement solutions for newbuilding vessels. Transport. Res. Transport Environ. 99, 102989.
Zverkhovskyi, O., De Jong, J., 2020. Damen air cavity system of sustainable passenger ships. In: Proceedings of the Intern. Conf.«Sustainable and Safe Passenger Ships».–Athens (Greece). Royal Institution of Naval Architects & Hellenic Institute of Marine Technology, pp. 65–70.